

Article

# Global and Local Analysis for a Cournot Duopoly Game with Two Different Objective Functions

Sameh Askar <sup>\*</sup>, Abdulaziz Foul , Tarek Mahrous, Saleh Djemele and Emad Ibrahim

Department of Statistics and Operations Research, College of Science, King Saud University, P.O. Box 2455, Riyadh 11451, Saudi Arabia; abdefoul@KSU.EDU.SA (A.F.); tmahrous@KSU.EDU.SA (T.M.); djemele@KSU.EDU.SA (S.D.); memad@ksu.edu.sa (E.I.)

\* Correspondence: saskar@ksu.edu.sa; Tel.: +966-555-88-3742

**Abstract:** In this paper, a Cournot game with two competing firms is studied. The two competing firms seek the optimality of their quantities by maximizing two different objective functions. The first firm wants to maximize an average of social welfare and profit, while the second firm wants to maximize their relative profit only. We assume that both firms are rational, adopting a bounded rationality mechanism for updating their production outputs. A two-dimensional discrete time map is introduced to analyze the evolution of the game. The map has four equilibrium points and their stability conditions are investigated. We prove the Nash equilibrium point can be destabilized through flip bifurcation only. The obtained results show that the manifold of the game's map can be analyzed through a one-dimensional map whose analytical form is similar to the well-known logistic map. The critical curves investigations show that the phase plane of game's map is divided into three zones and, therefore, the map is not invertible. Finally, the contact bifurcation phenomena are discussed using simulation.



**Citation:** Askar, S.S.; Foul, A.; Mahrous, T.; Djemili, S.; Ibrahim, E. Global and Local Analysis for a Cournot Duopoly Game with Two Different Objective Functions. *Mathematics* **2021**, *9*, 3119. <https://doi.org/10.3390/math9233119>

Academic Editor: Mikhail Goubko

Received: 9 October 2021

Accepted: 30 November 2021

Published: 3 December 2021

**Publisher's Note:** MDPI stays neutral with regard to jurisdictional claims in published maps and institutional affiliations.



**Copyright:** © 2021 by the authors. Licensee MDPI, Basel, Switzerland. This article is an open access article distributed under the terms and conditions of the Creative Commons Attribution (CC BY) license (<https://creativecommons.org/licenses/by/4.0/>).

**Keywords:** cobweb model; dynamics; gradient mechanism; stability; bifurcation

## 1. Introduction

The duopoly market structure has been deeply studied and investigated as a significant aspect of economic dynamics and game theory. This market consists of only two competing firms in which each firm selects its strategy based on its own actions and the actions of its competitor. In duopoly models, it is assumed that firms independently seek a level of production that maximizes their profits. That is, all competing firms decide their output productions simultaneously. Moreover, firms have the same visualization of the demand of the market and they have familiar insight into their competitors' operating costs. In such a duopoly game, all the competitors decide to be more productive. This means that a firm decides to update its output production depending on an increase or decrease in its production based on the gained profit. Game theory is categorized as a branch of applied mathematics, which refers to the process in which individuals or organizations can interact so that they can achieve corresponding benefits. Game theory has been adopted to study competitive behaviors amongst rivals and has been widely applied in management, biology, economics, and other disciplines. It has been used in investigating static duopoly models as well. The static models of this game may not provide more information or facts about the evolution of the game as they concentrate on the static Nash point. This means the competing firms in static models are not willing to change their strategic behaviors because they understand that deviation from the Nash point is useless. More information and studies on static models can be found in the literature [1–5].

Studying the dynamic characteristics of such games has given rise to some hidden behaviors of maps describing its evolution. The structure of these maps is discrete and depends on time steps. Examples of these hidden behaviors include stability, bifurcation, basin of attraction, and global bifurcation. The first step to investigating these behaviors is

the modeling process, which requires some assumptions for the inverse demand and cost functions. Several investigations in the literature have analyzed the dynamic characteristics of such models based on several types of inverse and cost functions including linear and nonlinear ones. The first trial was used for discussing [6] these dynamic characteristics of an oligopoly model. Another type of these games, called Cournot–Bertrand, was introduced and its dynamics behaviors were discussed in [7]. Puu ([8,9]), a famous scientist who passed away in 2020, studied the complex dynamics characteristics of many oligopoly games. His works have become a central point for many studies in the literature and provided this research field with several beneficial books and articles. Other studies in the literature ([10–18]) have analyzed market structure and kinds of market competitions, including several types of inverse demand and cost functions in addition to different strategies used by competing firms for productions updating. The above studies and others in the literature have reported that such games possess periodic, quasi-periodic, and complex attractors with peculiar structures that route to chaos.

The literature reports several studies in addition to those cited above focusing on a single-objective function to be maximized. This single-objective function was the firm's gained profit. Recently, few works on duopoly games have focused on maximizing another single-objective function: an average weighting of two objective functions. For example, the static game of quantity-setting was studied by Fanti et al. [19]. In this study, the authors analyzed the game's players that followed corporate social responsibility (CSR), which depended on managerial delegation. In [20], the weighted average between two objective functions, profit and social welfare, was maximized to seek the equilibrium points of Cournot–Bertrand model, whose productions are differentiated. Recalling the relation between R&D expenditure, a static duopoly game with players seeking to maximize their own and relative profits was investigated in [21]. Maximizing social welfare as a single-objective function of a Cournot duopoly game was analyzed and its dynamics were discussed [22]. Ref. [22] carried out an intensive local and global analysis for exploring the stability conditions of the Nash point and the types of bifurcations that lead this point to be unstable. Several investigations on a hybrid model of oligopoly with privatization policies and CSR have shown that the optimality of private policies are impacted by both CSR and the heterogeneity of private company objectives [23]. In [24], a multistability process was discussed in a two-stage production-setting duopoly game with differentiated products and R&D spillover. Recently, ref. [25] carried out an analysis of the Cournot duopoly model with players seeking the maximization of a weighted single objective of firm profit and consumer surplus.

Market information means information on quantity, quality, packaging, and/or prices of marketed, imported, and/or exported products. Such information can help firms to use an appropriate adjustment rule by which productions can be updated. Identifying the rule of adjustment can be used for the evolution of a game and for building a discrete time map responsible for describing the evolution. Several adjustment rules have been described in the literature for that purpose. For example, bounded rationality approach has been intensively adopted in several studies for the modeling process. It is considered a gradient approach based on the maximization of the marginal objective function. In addition, there are other rules that have been used in the modeling process and are reported in the literature, such as naïve expectation, the tit-for-tat rule, and the local monopolistic approximation (LMA) rule. For more information on the properties of such rules, the reader is referred to some works in the literature ([26–30]).

The current paper proposes a game of duopoly that belongs to the above discussed categories. Its players (or firms) seek optimal quantities of their productions according to the maximization of two different objective functions. The first firm wants to maximize a weighted objective function between its social welfare and profit. The second firm wants to maximize its relative profit. As in the literature, we adopt a simple linear price function in the modeling process. Then, the evolution of game is described by a nonlinear noninvertible map. It possesses four equilibrium points, one of which is interior and is

considered a Nash equilibrium point. We conduct a local and global analysis of these points and focus on the dynamics of the Nash point including its stability conditions, contact bifurcation, and attractive basins of some periodic cycles and chaotic attractors using numerical simulation experiments. The critical curves analysis shows the map of game belongs to the  $Z_4 - Z_2 - Z_0$  type.

The remainder of this paper is structured as follows: The model is introduced in Section 2. In Section 3, local analysis of the equilibrium points is discussed. The invariant manifold is investigated in Section 4, while the global bifurcation phenomena are discussed using numerical simulation in Section 5. The case of equal speed of adjustments is studied in Section 6. Finally, Section 7 concludes our findings.

## 2. The Model

Let us suppose two competing firms (or players) producing homogeneous commodities. These commodities represent the firms' decision variables and are set by  $q_1$  and  $q_2$ . The cost of production for each firm is taken as linear function in the form  $C_i(q_i) = c_i q_i, i = 1, 2$ , where  $c_i > 0, i = 1, 2$  is called the marginal cost ( $\frac{\partial C_i}{\partial q_i}, i = 1, 2$ ) and is constant. Both firms adopt a linear inverse demand function given by

$$p = g(Q) = a - bQ \quad (1)$$

where  $p$  is the price of production, the parameter  $b > 0$  is used to represent firms' sensitive price coefficient to their own productions, and  $Q = q_1 + q_2$  is the total supply by firms to the market. The parameter  $a > 0$  is set for the largest price in the market when  $q_1 = 0$  and  $q_2 = 0$ , which means that no productions of the two firms is provided to the market. The total profit by each firm is given by  $\pi_i = pQ - C_i(q_i), i = 1, 2$ ; so, using (1) we obtain

$$\pi_i = (a - c_i - bQ)q_i, a > c_i, i = 1, 2. \quad (2)$$

Unlike many studies in the literature, we examine the case when the two firms want to maximize two different objective functions. Due to the lack of market information provided to each firm (or competitor), the first firm seeks the maximization of its profit according to some social responsibility. Such responsibility, from an economic perspective, may be described by the social welfare ( $SW$ ) that is given by

$$SW = TR + CS. \quad (3)$$

where  $TR$  and  $CS$  represent total revenues and consumer surplus, respectively. The total revenue is equal to  $\pi_1 + \pi_2$  while  $CS$  is calculated by the following relation:

$$CS = \int_0^Q g(\bar{Q})d\bar{Q} - pQ = \frac{b}{2}Q^2; \bar{Q} \in (0, Q) \quad (4)$$

Substituting (1) and (5) in (3), we obtain,

$$SW = aQ - c_1q_1 - c_2q_2 - \frac{b}{2}Q^2. \quad (5)$$

So, the first firm wants to maximize the following weighted-sum objective,

$$f_1 = (1 - \omega)SW + \omega\pi_1 \quad (6)$$

where the parameter  $\omega$  denotes a certain weight and is restricted to the interval  $\omega \in [0, 1]$ . At  $\omega = 1$ , the first firm focuses on maximizing its profit only, as in many studies in the literature, and  $\omega = 0$  means that it focuses only on the social welfare, which economically may put it at risk. On the other hand, the second firm seeks maximization of its relative profit given by  $f_2 = \pi_2 - \epsilon\pi_1$  and  $\epsilon \in [0, 1]$ . At  $\epsilon = 0$ , the second firm concentrates on

maximizing its profit only and  $\epsilon = 1$  means it focuses on maximizing its relative profit. Now, the following two objective functions take the form

$$\begin{aligned} f_1 &= (1 - \omega) \left( aQ - c_1q_1 - c_2q_2 - \frac{b}{2}Q^2 \right) + \omega q_1(a - c_1 - bQ), \\ f_2 &= (a - c_2 - bQ)q_2 - \epsilon q_1(a - c_1 - bQ) \end{aligned} \tag{7}$$

So, the marginal objectives  $\left( \frac{\partial f_i}{\partial q_i}, i = 1, 2 \right)$  can be

$$\begin{aligned} \frac{\partial f_1}{\partial q_1} &= a - c_1 - (1 - \omega)bq_1 - bq_2, \\ \frac{\partial f_2}{\partial q_2} &= a - c_2 - 2bq_2 - (1 - \epsilon)bq_1 \end{aligned} \tag{8}$$

The market possesses many characteristics that can support firms with information about their output updates; such information is not complete but provides firms expectations about their rivals' decisions. Complete information is rare and if it exists, it may affect the firms' profits as it requires increased costs for collecting data. So, due to the limited information on the market, firms must be rational and estimate their marginal objective for updating their production in the next period in the production cycle. This means that if  $\frac{\partial f_i}{\partial q_i} > 0; i = 1, 2$ , both firms will provide the market with extra production in the next time period; otherwise, they may reduce their production. This discussion about updating firm production can be described by the bounded rationality rule [26–30] given by

$$q_i(t + 1) = q_i(t) + k_i(q_i) \frac{\partial f_i}{\partial q_i}; i = 1, 2 \tag{9}$$

The function  $k_i(q_i)$  may be used to measure a range on which a firm's production can be varied depending on the sign of the marginal objective. Here, we follow many studies in the literature and take it as  $k_i(q_i) = v_i q_i; i = 1, 2$  and  $v_i > 0, i = 1, 2$ . This means that  $\frac{q_i(t+1) - q_i(t)}{q_i(t)} \propto \frac{\partial f_i}{\partial q_i}$ ; hence, there is a direct proportional relationship between the relative production and the marginal objective function. Substituting (8) into (9), a nonlinear two-dimensional discrete dynamic map that is used to describe the game's evolution is obtained.

$$T(q_1, q_2): \begin{cases} q_1(t + 1) = q_1(t) + v_1 q_1(t)(a - c_1 - (1 + \omega)bq_1 - bq_2), \\ q_2(t + 1) = q_2(t) + v_2 q_2(t)(a - c_2 - 2bq_2 - (1 - \epsilon)bq_1) \end{cases} \tag{10}$$

The parameter  $t, t = 0, 1, 2, \dots$  denotes the time steps. Inputting the condition for fixed points  $T(q_1, q_2) = (q_1, q_2)$  into (10), we obtain four fixed points given by

$$\begin{aligned} e_0 &= (0, 0), \\ e_1 &= \left( \frac{a - c_1}{b(1 + \omega)}, 0 \right), e_2 = \left( 0, \frac{a - c_2}{2b} \right) \\ e_* &= (\bar{q}_1, \bar{q}_2) = \left( \frac{a - 2c_1 + c_2}{b(1 + \epsilon + 2\omega)}, \frac{a(\epsilon + \omega) + (1 - \epsilon)c_1 - (1 + \omega)c_2}{b(1 + \epsilon + 2\omega)} \right) \end{aligned} \tag{11}$$

We can see that  $e_1, e_2$  and the Nash point  $e_*$  are positive points.

### 3. Local Analysis

In order to investigate the local stability of the above fixed points, we must recall the Jacobian matrix for map (10) as follows:

$$J(q_1, q_2) = \begin{bmatrix} 1 + v_1(a - c_1 - 2b(1 + \omega)q_1 - bq_2) & -bv_1q_1 \\ -b(1 - \epsilon)v_2q_2 & 1 + v_2(a - c_2 - 4bq_2 - b(1 - \epsilon)q_1) \end{bmatrix} \tag{12}$$

It is clear that (10) is a 2D map and then (12) has two eigenvalues,  $\lambda_1$  and  $\lambda_2$ , corresponding to each fixed point. This means that a fixed point is stable if  $|\lambda_i| < 1, i = 1, 2$ . Now, the following propositions are raised (see the proofs in Appendix A):

**Proposition 1.** *The point  $e_0$  is an unstable node.*

**Proposition 2.** *The point  $e_1$  possesses two possibilities:*

- *It is a saddle point if  $0 < v_1 < \frac{2}{(a-c_1)}$  and  $\lambda_2 > 1$ .*
- *It is an unstable node if  $v_1 > \frac{2}{(a-c_1)}$ .*

The stability of  $e_2$  is the same as that of  $e_1$ . It is saddle provided that  $0 < v_2 < \frac{2}{(a-c_2)}$  and  $\lambda_2 > 1$  and unstable node provided that  $v_2 > \frac{2}{(a-c_2)}$ . From an economic point of view, it is known that  $e_0$  represents a bankrupting financial issue affecting each firm. The two points  $e_1$  and  $e_2$  represent a monopoly case; one firm dominates the market and the other one leaves it.

**Proposition 3.** *The point  $e_*$  is stable if*

$$0 < \frac{-(a - 2c_1 + c_2)[a(\epsilon + \omega) - 2(1 + \omega)c_2 + (1 - \epsilon)c_1]v_1v_2}{1 + \epsilon + 2\omega} + \frac{2(1 + \omega)(a - 2c_1 + c_2)v_1 - 4[(1 + \omega)c_2 - (1 - \epsilon)c_1 - a(\epsilon + \omega)]v_2}{1 + \epsilon + 2\omega} < 4 \tag{13}$$

According to the jury conditions given in (A6), the Nash point becomes stable under condition (13). In order to confirm this theoretical result, we must plot the region of the Nash stability and instability as shown in Figure 1a, depicted by the values of parameters  $a = 0.9, b = 0.8, c_1 = 0.3, c_2 = 0.4, \epsilon = 0.2$  and  $\omega = 0.95$  in the  $(v_1, v_2)$  plane. It presents the region in which flip bifurcation can only exist.

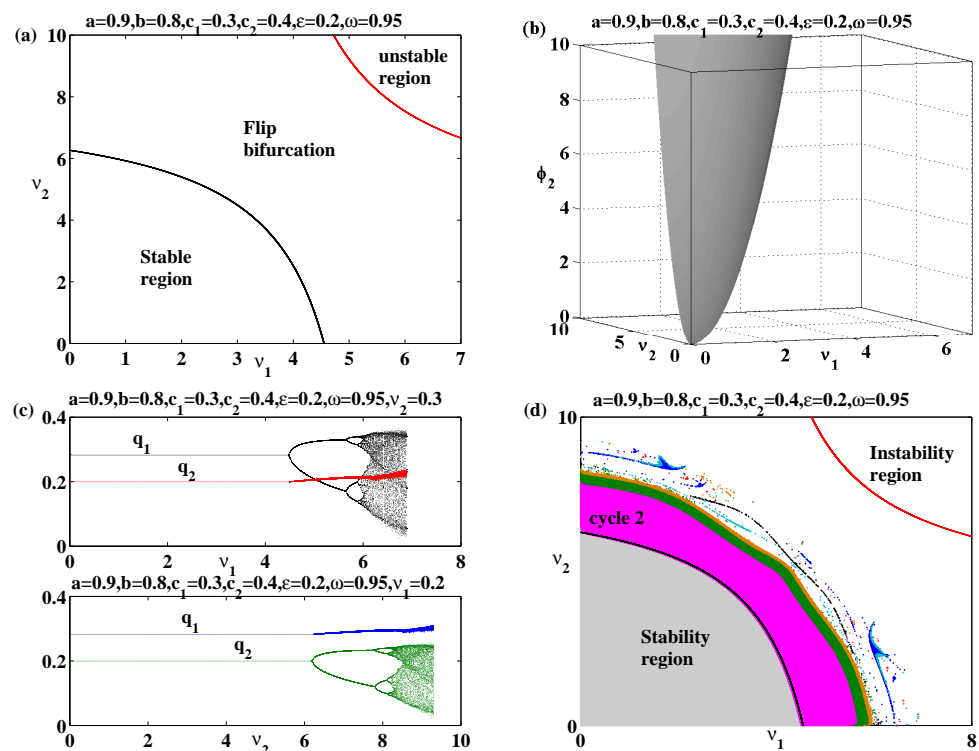


**Figure 1.** (a) Stability region of the Nash point in the  $(v_1, v_2)$  plane at:  $a = 0.9, b = 0.8, c_1 = 0.3, c_2 = 0.4, \epsilon = 0.2$  and  $\omega = 0.95$ . (b) The value of  $\phi_2$  at:  $a = 0.9, b = 0.8, c_1 = 0.3, c_2 = 0.4, \epsilon = 0.2$ , and  $\omega = 0.95$ . (c) The 1D bifurcation diagrams with varying  $v_1$  and  $v_2$ . (d) The 2D bifurcation diagram on the  $(v_1, v_2)$  plane.

**Proposition 4.** *The Nash point can be destabilized due to flip bifurcation only.*

As it can be seen that  $\phi_2$  in (A7) depends on several parameters, some numerical experiments were carried out to confirm that it is a non-negative value. At the parameters values  $a = 0.9, b = 0.8, c_1 = 0.3, c_2 = 0.4, \epsilon = 0.2$ , and  $\omega = 0.95$ , it is clear that this value is non-negative, as plotted in Figure 1b. This also confirms that Neimark–Sacker does not occur. Other simulation experiments for different values of those parameters confirmed that we can only obtain Jacobian (12) at the Nash point of two real eigenvalues. Our obtained results indicate that the point  $e_*$  is locally stable within a certain interval in the speed of adjustments  $(v_1, v_2)$  plane. Then, it becomes unstable due to flip bifurcation. So, we performed some numerical simulations in order to investigate the influences of these adjustment parameters on the map’s dynamics. Let us fix the parameters values to  $a = 0.9, b = 0.8, c_1 = 0.3, c_2 = 0.4, \epsilon = 0.2, v_2 = 0.3$ , and  $\omega = 0.95$ . Figure 1c depicts the 1D bifurcation diagram with varying  $v_1$ . As shown, the Nash point becomes stable until it reaches the value of  $v_1$ , where the period-2 cycle starts and then followed by other high periodic cycles, and routes to chaos exist. The same result can be obtained by varying the parameter  $v_2$  at the parameters values  $a = 0.9, b = 0.8, c_1 = 0.3, c_2 = 0.4, \epsilon = 0.2, v_1 = 0.2$ , and  $\omega = 0.95$ , as shown in Figure 1c. In Figure 1d, the 2D bifurcation diagram presents the stable region of the Nash point colored in gray, while the other colors denote the period 2 cycle and higher periodic cycles. It is plotted with the parameters values  $a = 0.9, b = 0.8, c_1 = 0.3, c_2 = 0.4, \epsilon = 0.2$ , and  $\omega = 0.95$ . Furthermore, the simulation experiments with these values showed that the 1D bifurcation diagrams depicted in Figure 1c confirm the stability of the Nash point when the following conditions are imposed on the speed parameters:  $0 < v_1 < 4.4957$  and  $0 < v_2 < 6.2040$ . Above these restrictions on  $v_1$  and  $v_2$ , the period 2 cycles appear to be followed by higher periodic cycles through flip bifurcation.

#### 4. The Invariant Manifold

The map  $T$  defined in (10) has a trapping point, which is the origin  $(0, 0)$ . The trapping point means that  $q_1(t) = 0$  or  $q_2(t) = 0$  makes  $q_1(t + 1) = 0$  or  $q_2(t + 1) = 0$ . That is, the coordinate axes  $q_1$  and  $q_2$  are invariant axes for the map  $T$ . So, the invariant set made of axis  $q_1$  (and  $q_2$ ) forms an invariant manifold for  $T$ . Now, substituting  $q_1 = 0$  in (10) produces

$$q_1(t + 1) = (1 + (a - c_1)v_1)q_1(t) \left[ 1 - \frac{b(1 + \omega)v_1}{1 + (a - c_1)v_1} q_1(t) \right] \tag{14a}$$

and substituting  $q_2 = 0$  in (10) provides

$$q_2(t + 1) = (1 + (a - c_2)v_2)q_2(t) \left[ 1 - \frac{2bv_2}{1 + (a - c_2)v_2} q_2(t) \right] \tag{14b}$$

One can see that (14a) and (14b) are topologically equivalent to

$$u_i(t + 1) = \mu_i u_i(t)(1 - u_i(t)) , i = 1, 2 \tag{15}$$

depending on the following transformations

$$\begin{aligned} q_1 &= \frac{1 + (a - c_1)v_1}{b(1 + \omega)v_1} u_1, \\ q_2 &= \frac{1 + (a - c_2)v_2}{2bv_2} u_2 \end{aligned} \tag{16}$$

and  $\mu_i = 1 + (a - c_i)v_i, i = 1, 2$ . This indicates that analyzing the dynamics of trajectories for the map  $T$  that commence at  $q_1$  (or  $q_2$ ) can be investigated from maps (14a) or (14b).

##### 4.1. Dynamic Analysis (Monopoly Case)

Let us start with (14a), which can be rewritten as

$$\sigma(u) = \mu_1 u(1 - u) \tag{17}$$

Equation (17) represents a logistic map and the parameter  $\mu_1$  is responsible for its dynamics. The function  $\sigma(u)$  has a derivative,  $\sigma'(u) = \mu_1(1 - 2u)$ . Setting  $\sigma'(u) = 0$  gives the point  $u = 1/2$  and, hence,  $\sigma(u)$  has its maximum value,  $\mu_1/4$ . Furthermore,  $\sigma(0) = 0$  and  $\sigma(1) = 0$ , which means that restricting  $\mu_1$  in  $(0, 4)$  imposes  $\sigma(u) \in [0, 1]$  for all  $u \in [0, 1]$ . In addition, qw can see that map (15) has two fixed points,  $\bar{u} = 0$  and  $\bar{u} = 1 - \frac{1}{\mu_1}$  and  $\mu_1 > 1$ . So,  $\sigma'(0) = \mu_1$ , and then  $\bar{u} = 0$  is stable if  $\mu_1 \in (0, 1)$ , and unstable otherwise. The other fixed point,  $\bar{u} = 1 - \frac{1}{\mu_1}$ , is stable if  $\mu_1 \in (1, 3)$  and unstable if  $\mu_1 > 3$ . The same discussion and analysis can be carried out for map (14b). The numerical simulation shown in Figure 2a is a 1D bifurcation diagram with respect to the parameter  $\mu$ , which confirms that the fixed point  $\bar{u} = 1 - \frac{1}{\mu_1}$  is stable in the interval  $\mu_1 \in (1, 3)$ . In Figure 2b, the cobweb diagram is plotted for the value  $\mu_1 = 2.99$  in the interval of stability and shows a stable fixed point; in Figure 2c, it is plotted at the value  $\mu_1 = 3.75$ , which lies in the instability region, thereby confirming the instability of the fixed point. The same discussion and analysis can be obtained for map (14b).

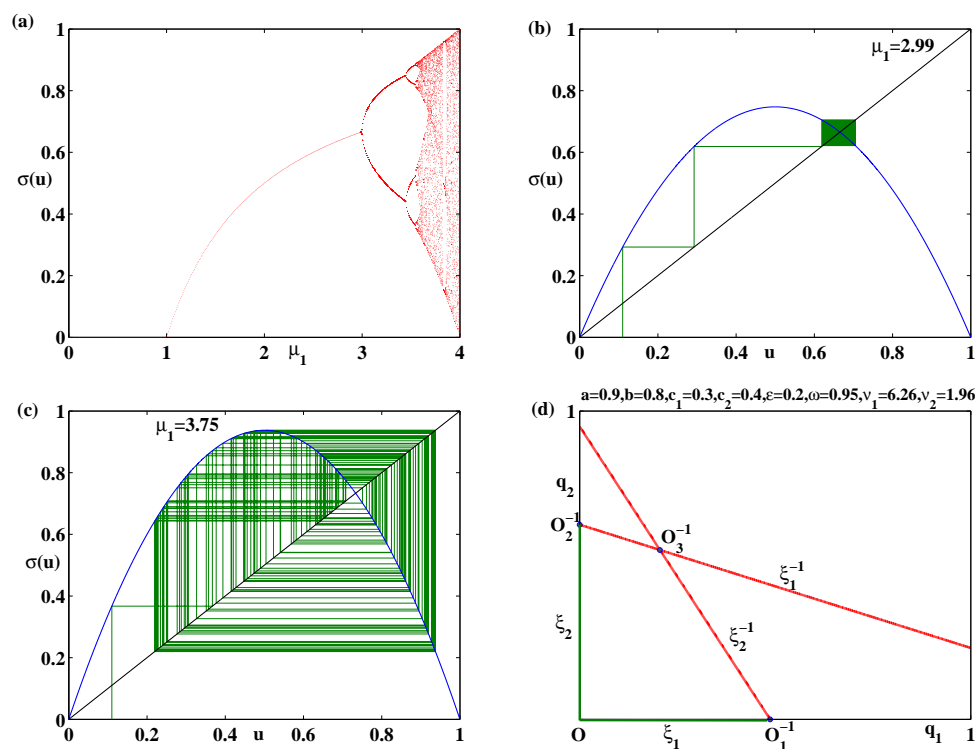


**Figure 2.** (a) The 1D bifurcation diagram of map  $\sigma(u)$  with respect to  $\mu_1$ . Iterations of  $\sigma(u)$  at (b)  $\mu = 2.99$  and (c)  $\mu = 3.75$ . (d) The lines  $\xi_1$  and  $\xi_2$  and their inverses at:  $a = 0.9, b = 0.8, c_1 = 0.3, c_2 = 0.4, \epsilon = 0.2, \omega = 0.95, v_1 = 6.26, v_2 = 1.96$ .

**Proposition 5.** *If the critical value  $v_i = \frac{2}{(a-c_i)}, i = 1, 2$  exists, then the trajectories of  $T$  on the invariant axes diverge when  $v_i \in \left(\frac{2}{(a-c_i)}, +\infty\right), i = 1, 2$ .*

**Proof.** The above discussion confirms the topological equivalence between the map  $T$  given in (10) with (14a) and (14b), and hence the trajectories of (14a) or (14b) are divergent if  $\mu_i > 3, i = 1, 2$ . The proof is straightforward as  $\mu_i = 1 + (a - c)v_i$ .  $\square$

4.2. Basin of Attraction

The topological structure of the basin of attraction was studied to explore the phase plane of the map’s dynamics. Following to Cavalli [17] and Fanti [19], it possible to analyze coordinate axes and their preimages of any rank from the boundaries for any initial state of any nondiverging trajectory.

Suppose that  $H \subset \mathbb{R}^2$  refers to an attractor for  $T$ , and let there exist a neighborhood  $V$  of  $H$  such that  $T(V) \in V$  and  $T^{(m)}(q_1, q_2) \rightarrow H$  as  $m \rightarrow \infty$  and  $(q_1, q_2) \in V$ . Then, the basin of attraction  $H$  denoted by  $B(H)$  is defined as the set of all points whose orbits in  $H$  converge to  $H$  after a finite number of iterations. That is,

$$B(H) = \left\{ (q_1(0), q_2(0)) \mid T^{(m)}(q_1(0), q_2(0)) \rightarrow H, m \rightarrow \infty \right\}$$

Conversely, the infinite basin of attraction that is denoted by  $B(\infty)$  is defined as a domain whose points form a divergent locus. Investigating  $B(H)$  requires us to first calculate its boundary,  $\partial B(H)$ . Therefore, let  $F$  refer to a boundary that separates the two basins  $B(H)$  and  $B(\infty)$ ; then,  $F = \partial B(H) = \partial B(\infty)$ . The above discussion on the map  $T$  shows that  $(0, 0)$  is a trapping point and the coordinate axes  $q_1$  and  $q_2$  form an invariant manifold. Furthermore, the dynamics of  $T$  on those axes can be studied using both (14a) and (14b), which can be rewritten by

$$\begin{aligned} \dot{q}_1 &= g_1(q_1) = q_1 + v_1 q_1(a - c_1 - (1 + \omega)bq_1), \\ \dot{q}_2 &= g_2(q_2) = q_2 + v_2 q_2(a - c_2 - 2bq_2) \end{aligned} \tag{18}$$

that has the two positive fixed points,  $\bar{q}_1 = \frac{a-c_1}{b(1+\omega)}$  and  $\bar{q}_2 = \frac{a-c_2}{2b}$ . If  $v_i(a - c_i) < 1, i = 1, 2$ , then  $g_i$  is an increasing concave function and for any  $q_1 > 0, q_2 = 0$  (resp.  $q_1 = 0, q_2 > 0$ ), we obtain  $\dot{q}_1 > 0, \dot{q}_2 = 0$  (resp.  $\dot{q}_1 = 0, \dot{q}_2 > 0$ ). On the other hand, if  $v_i(a - c_i) > 1, i = 1, 2$ , then  $g_i$  is concave and a unimodal function. Letting  $\dot{q}_i = 0, g_i = 0, i = 1, 2$ , we obtain  $\hat{q}_1^{bo} = \frac{1+v_1(a-c_1)}{bv_1(1+\omega)}, \hat{q}_2^{bo} = \frac{1+v_2(a-c_2)}{2bv_2}, \hat{q}_1^{cr} = \frac{1+v_1(a-c_1)}{2bv_1(1+\omega)}, \hat{q}_2^{cr} = \frac{1+v_2(a-c_2)}{4bv_2}$ , which are non-negative points. If  $g_i(\hat{q}_i^{cr}) < \hat{q}_i^{bo}$ , i.e., if  $v_i < \frac{2}{(a-c_i)}, i = 1, 2$ , then bounded trajectories on invariant axes  $q_1$  and  $q_2$  are obtained provided that the initial state of map (18) lies on the line segment  $\xi_i = [O, O_i^{-1}], i = 1, 2$ , where  $O_i^{-1}, i = 1, 2$  is the rank 1 preimage corresponding to each axis and is given by

$$\begin{aligned} O_1^{-1} &= \hat{q}_1^{bo} = \frac{1 + v_1(a - c_1)}{bv_1(1 + \omega)}, \\ O_2^{-1} &= \hat{q}_2^{bo} = \frac{1 + v_2(a - c_2)}{2bv_2} \end{aligned}$$

In contrast, for initial states beginning outside  $\xi_i, i = 1, 2$ , their trajectories diverge (become infeasible) to infinity as time goes to infinity. For the points in the form  $(p, 0) \in \xi_1, (0, q) \in \xi_2$ , where  $0 < p < \hat{q}_1^{bo}$  and  $0 < q < \hat{q}_2^{bo}$ , their rank 1 preimages denoted by  $\xi_i^{-1} = T^{-1}(\xi_i), i = 1, 2$  can be obtained by algebraically solving the following:

$$\begin{aligned} q_1(t) + v_1 q_1(t)(a - c_1 - (1 + \omega)bq_1 - bq_2) &= p, \\ q_2(t) + v_2 q_2(t)(a - c_2 - 2bq_2 - (1 - \epsilon)bq_1) &= 0 \end{aligned} \tag{19}$$

and

$$\begin{aligned} q_1(t) + v_1 q_1(t)(a - c_1 - (1 + \omega)bq_1 - bq_2) &= 0, \\ q_2(t) + v_2 q_2(t)(a - c_2 - 2bq_2 - (1 - \epsilon)bq_1) &= q \end{aligned} \tag{20}$$

Solving (19) and (20) results in

$$\begin{cases} \xi_1 : q_2 = 0, \\ \xi_1^{-1} : 1 + v_2[a - c_2 - 2bq_2 - (1 - \epsilon)bq_1] = 0 \end{cases} \tag{21}$$

$$\begin{cases} \xi_2 : q_1 = 0, \\ \xi_2^{-1} : 1 + v_1[a - c_1 - (1 + \omega)bq_1 - bq_2] = 0 \end{cases} \tag{22}$$

Solving (21) and (22) algebraically produces two rank 1 preimages. These preimages are  $\xi_1$  (and  $\xi_2$ ), and their inverses are  $\xi_1^{-1}$  (and  $\xi_2^{-1}$ ). Due to the complicated forms of these points, some numerical simulations were investigated. Figure 2d depicts these lines and

their preimages at  $a = 0.9, b = 0.8, c_1 = 0.3, c_2 = 0.4, \epsilon = 0.2, \omega = 0.998, v_1 = 6.26$ , and  $v_2 = 1.96$ . We can see that  $\xi_1^{-1}$  intersects the axis ( $q_1 = 0$ ) in  $O_2^{-1}$ , and  $\xi_2^{-1}$  intersects the axis ( $q_2 = 0$ ) in  $O_1^{-1}$ , but they intersect at the point  $O_3^{-1}$ . These points,  $O, O_1^{-1}, O_2^{-1}$ , and  $O_3^{-1}$ , are the rank 1 preimages of the origin point. They take the form

$$O = (0, 0), O_1^{-1} = \left( \frac{1 + v_1(a - c_1)}{bv_1(1 + \omega)}, 0 \right), O_2^{-1} = \left( 0, \frac{1 + v_2(a - c_2)}{2bv_2} \right)$$

$$O_3^{-1} = \left( \frac{(a - 2c_1 + c_2)v_1v_2 - v_1 + 2v_2}{b(1 + \epsilon + 2\omega)v_1v_2}, \frac{[(1 - \epsilon)c_1 - (1 + \omega)c_2 + (\epsilon + \omega)a]v_1v_2 - (1 - \epsilon)v_2 + (1 + \omega)v_1}{b(1 + \epsilon + 2\omega)v_1v_2} \right)$$

It is clear that the origin point has a four real rank 1 preimages, as shown above. This means the origin belongs to the  $Z_4$  zone, the zone possessing four different rank 1 preimages. Figure 3a shows these points with a chaotic attractor denoted by  $H$  occurring at the parameters values  $a = 0.9, b = 0.8, c_1 = 0.3, c_2 = 0.4, \epsilon = 0.2, \omega = 0.998, v_1 = 6.26$ , and  $v_2 = 1.96$ . It can also be seen that these points form a quadrilateral shape  $OO_1^{-1}O_2^{-1}O_3^{-1}$  that contains this attractor and its attracting domain denoted by  $B(H)$  in white, while the infeasible domain is denoted by  $B(\infty)$  in gray. Furthermore, the line segments  $\xi_1^{-1}$  and  $\xi_2^{-1}$  separate these two domains. The figure also shows that some parts from the infeasible domain are located in the attracting domain, and then the infeasible domain converts from a connecting set to disconnecting one. In order to investigate this phenomenon, we need to calculate the critical curves.

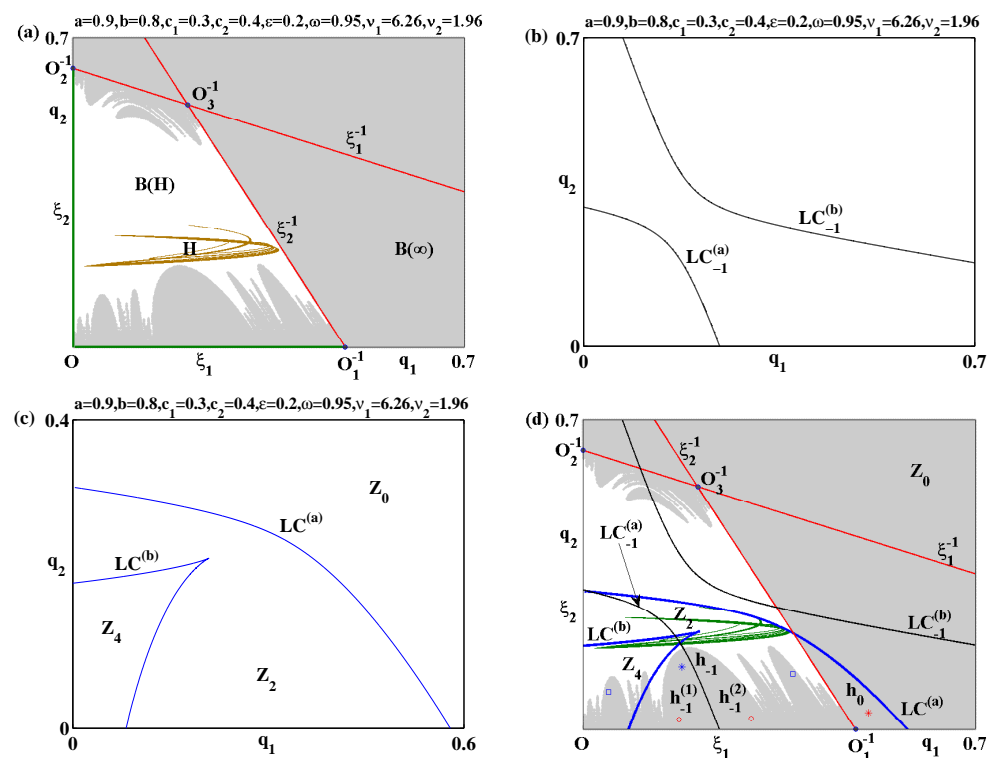


**Figure 3.** At the parameter values of  $a = 0.9, b = 0.8, c_1 = 0.3, c_2 = 0.4, \epsilon = 0.2, \omega = 0.998, v_1 = 6.26$  and  $v_2 = 1.96$ . (a) Basin of attraction for a chaotic attractor. (b) The two branches of  $LC_{-1}$ . (c) The two branches of  $LC$ . (d) The change in the shape of  $B(\infty)$  from a connecting set to a disconnecting one for a chaotic attractor.

### 4.3. Critical Curves

For further visualization of the fractal structure of the attractive basin, one has to study the critical curves and their characteristics. These curves are important as they provide a better explanation of this structure. They were studied in detail in [8]. The above discussion shows that the map  $T$  is a many-to-one map. That means any an unknown point in the form

$(p, 0)$  or  $(0, q)$  may own two real rank 1 preimages. In addition, the point  $(0, 0)$  has four different real rank 1 preimages. For points other than those, there may exist no preimages or more than two preimages. Consequently, the map  $T$  is a noninvertible map and belongs to the  $Z_4 - Z_2 - Z_0$  type, where  $Z_i, i = 0, 2, 4$  divides its phase plane. The zone  $Z_0$  contains no real rank 1 preimages, while the zone  $Z_2$  contains two different rank 1 preimages. The critical curve is used to separate these zones from each other; it is denoted by  $LC$  and separates zone whose number of preimages is equal. To calculate  $LC$ , we first must calculate  $LC_{-1}$ , which increases as the determinant of the Jacobian (12) decreases. It gives a hyperbola curve in the coordinates  $(q_1, q_2) \in \mathbb{R}^2$ . An iteration of these coordinates using the map  $T$ ,  $LC$  ( $LC = T(LC_{-1})$ ) forms the critical curve. Some numerical simulations were used to define both  $LC$  and  $LC_{-1}$ . At  $a = 0.9, b = 0.8, c_1 = 0.3, c_2 = 0.4, \epsilon = 0.2, \omega = 0.998, \nu_1 = 6.26$ , and  $\nu_2 = 1.96$ , Figure 3b shows that  $LC_{-1}$  consists of two branches,  $LC_{-1}^{(a)}$  and  $LC_{-1}^{(b)}$ . With the same set of values, Figure 3c depicts the critical curve  $LC$ , which also consists of two branches,  $LC^{(a)}$  and  $LC^{(b)}$ . We can see that  $Z_4, Z_2$  and  $Z_0$  divide the phase plane and are separated by the two branches of  $LC$ .

## 5. Global Bifurcation

It was shown above that the nonlinear map (10) is not invertible and its phase plane is divided into three zones. Now, we investigate an important aspect for this map, which is called global bifurcation. Different numerical simulation experiments on the map were performed given that it possesses a contact bifurcation. This kind of bifurcation occurs when there exists a contact between the critical curves and the boundaries of infinite basin of attraction  $\partial B(\infty)$ . It causes a change in the shape of  $B(\infty)$ , which changes it from a connecting set to a disconnecting one, as shown in Figure 3d, in which gray holes belong to  $B(\infty)$ , which are located in the attracting domain. To make this visible, let us assume the set of values,  $a = 0.9, b = 0.8, c_1 = 0.3, c_2 = 0.4, \epsilon = 0.2, \omega = 0.998, \nu_1 = 6.26$ , and  $\nu_2 = 1.96$ . As shown in Figure 3d, the basin of attraction of the chaotic attractor given in Figure 4a is distributed along the three zones. Additionally, a region of the infinite domain  $B(\infty)$  enters from the  $Z_0$  zone to  $Z_2$  and is denoted by  $h_0$ . It is located between  $\xi_2^{-1}$  and  $LC^{(a)}$  and its points possess two distinct real preimages. These preimages also belong to the infinite basin of attraction. All points belonging to  $h_0$  are responsible for creating the main hole  $h_{-1}$  embedded in the attracting domain. This hole consists of two areas,  $h_{-1}^{(1)}$  and  $h_{-1}^{(2)}$ , which are connected by  $LC_{-1}^{(a)}$ . The hole is entirely located in the  $Z_2$  zone. Every point belonging to this main hole possesses two distinct real preimages and is responsible for forming small holes belonging to  $B(\infty)$  and in both zones  $Z_2$  and  $Z_4$ . This is clarified in Figure 3d, where points belonging to  $h_0$  such as the red star point has two real rank 1 preimages denoted by a red circle in  $h_{-1}^{(1)}$  and  $h_{-1}^{(2)}$ ; hence, these points construct the main hole located in  $Z_2$ . Moreover, points belonging to the main hole  $h_{-1}$ , such as the blue star point, are responsible for forming points in the small holes, such as the two blue square points. Consequently, contact bifurcation exists and gives rise to disconnection in  $B(\infty)$ .

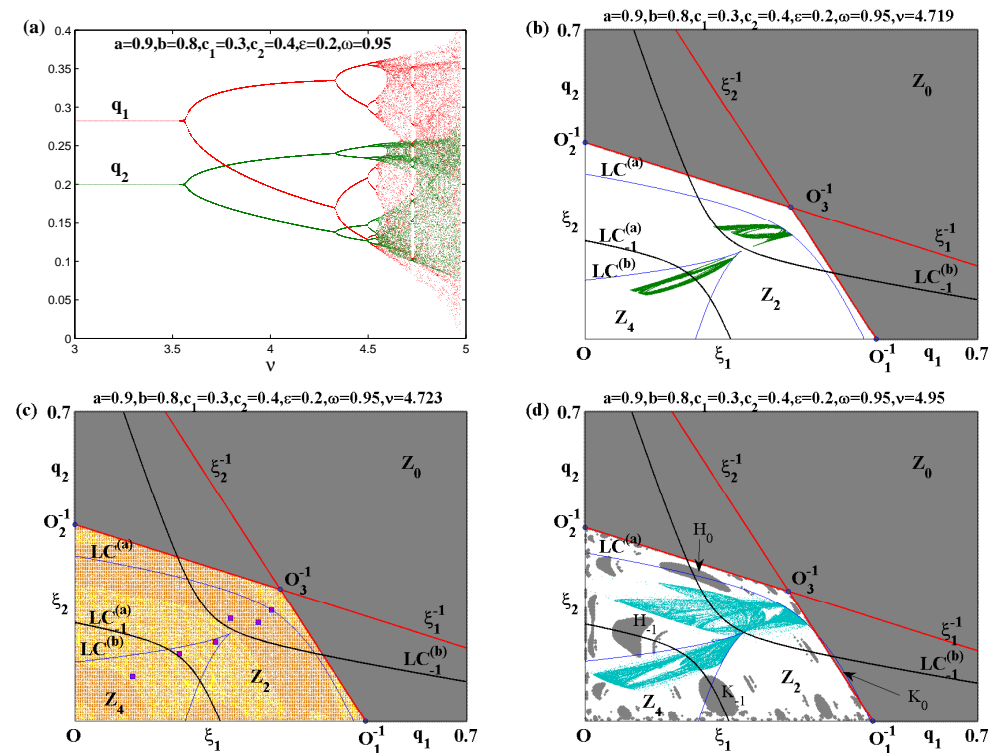


**Figure 4.** (a) A 1D bifurcation diagram with respect to  $\nu$  at  $a = 0.9, b = 0.8, c_1 = 0.3, c_2 = 0.4, \epsilon = 0.2, \omega = 0.998$ . The attractive basin at  $a = 0.9, b = 0.8, c_1 = 0.3, c_2 = 0.4, \epsilon = 0.2, \omega = 0.998$ , for (b) a two-bands chaotic attractor at  $\nu = 4.719$ , (c) period 6 cycle at  $\nu = 4.723$ , and (d) one piece chaotic attractor at  $\nu = 4.95$ .

### 6. Equal Speed of Adjustments

Let us suppose  $\nu_1 = \nu_2 = \nu$  represents the case of equal adjustment parameters. The map  $T$  then becomes

$$T_*(q_1, q_2): \begin{cases} q_1(t+1) = q_1(t) + \nu q_1(t)(a - c_1 - (1 + \omega)bq_1 - bq_2), \\ q_2(t+1) = q_2(t) + \nu q_2(t)(a - c_2 - 2bq_2 - (1 - \epsilon)bq_1) \end{cases} \quad (23)$$

The influences of the speed of adjustment parameter  $\nu$  was tested using numerical simulation. Assuming  $a = 0.9, b = 0.8, c_1 = 0.3, c_2 = 0.4, \epsilon = 0.2, \omega = 0.998$ , Figure 4a shows a 1D bifurcation diagram with respect to this parameter. We can see that the Nash point is stable until the increase in the period 2 cycle where flip bifurcation exists. It is also clear that the two competing firms are not synchronized. In Figure 4b, the simulation gives rise to a chaotic attractor that consists of two bands at the parameter values  $a = 0.9, b = 0.8, c_1 = 0.3, c_2 = 0.4, \epsilon = 0.2, \omega = 0.998$ , and  $\nu = 4.719$ . The basin of attraction of this chaotic attractor does not have any holes from the infinite basin, and the infinite basin forms a connecting set. As  $\nu$  increases to 4.723, we obtain a period 6 cycle that is given in Figure 4c with the basin of attraction of the Nash point. As we can see, the branch  $LC^{(a)}$  of the critical curve points upward. Numerical experiments showed that further increasing the speed parameter makes this branch tangential to the boundaries of the infinite basin of attraction; therefore, contact bifurcation occurs. It can be also seen that the basin of attraction of this cycle is included in the quadrilateral shape whose sides are  $\xi_1, \xi_2$  and their inverses  $\xi_1^{-1}, \xi_2^{-1}$ . At  $a = 0.9, b = 0.8, c_1 = 0.3, c_2 = 0.4, \epsilon = 0.2, \omega = 0.998$ , and  $\nu = 4.95$ ; a chaotic attractor with its basin of attraction is given in Figure 4d. We can see that the infinite basin of attraction becomes a disconnected set and holes are raised. There is also an area from the infinite basin denoted by  $K_0$  that enters from zone  $Z_0$  to zone  $Z_2$ . So, the points in this area belong to the area  $K_0$  and possess two distinct real rank 1 preimages. Moreover, this area is formed by two parts that are connected by the

branch  $LC_{-1}^{(b)}$ . In addition, there is an area denoted by  $H_0$  that is connected by the same branch of the critical curve and belongs to zones  $Z_0$  to  $Z_2$ . The points belonging to  $K_0$  and  $H_0$  are responsible for constructing the two different main holes denoted by  $K_{-1}$  and  $H_{-1}$ , as shown in Figure 4d. It can be seen that these main holes are connected by the branch  $LC_{-1}^{(a)}$ . The points belonging to these two holes are used to create the small holes near to the horizontal and vertical axes. It is also clear that the branch  $LC^{(a)}$  passes through the point  $O_1^{-1}$  and all the holes including the main one become tangents to the two axes  $q_1$  and  $q_2$ .

### 7. Conclusions

Some important dynamic characteristics such as stability, invariant manifold and global bifurcation for a duopoly game whose players adopt two different objective functions were analyzed in this manuscript. The obtained results showed that the Nash point can be destabilized through flip bifurcation only. Furthermore, the invariant manifold analysis showed that the dynamics of the two-dimensional map describing the duopoly game can be studied using a one-dimensional map that is similar to the well-known logistic map. In addition, the global analysis showed that there is a contact bifurcation occurring in the case of equal speed of adjustment parameters and gives rise to holes from the infinite basin of attraction located in the attracting domain of some chaotic attractors. Such holes may affect the evolution prediction if the initial states of the firms were selected from those holes. Moreover, we observed that the adjusting parameters affect the dynamics of the game in the long term. Finally, we found that adopting a high weight for profit may decrease the firm’s social welfare.

**Author Contributions:** Conceptualization, S.A.; methodology, S.A.; software, S.A.; validation, S.A., A.F., T.M., S.D. and E.I.; formal analysis, S.A.; investigation, S.A.; resources, S.A.; data curation, S.A.; writing—original draft preparation, S.A., A.F., T.M., S.D. and E.I.; writing—review and editing, S.A., A.F., T.M., S.D. and E.I.; visualization, S.A., A.F., T.M., S.D. and E.I.; supervision, S.A.; project administration, S.A.; funding acquisition, S.A. All authors have read and agreed to the published version of the manuscript.

**Funding:** Research Supporting Project number (RSP-2021/167), King Saud University, Riyadh, Saudi Arabia.

**Institutional Review Board Statement:** Not applicable.

**Informed Consent Statement:** Not applicable.

**Data Availability Statement:** The data is included in the paper.

**Conflicts of Interest:** The authors declare no conflict of interest.

### Appendix A

**Proof of Proposition 1.** Inputting  $e_0 = (0, 0)$  in (12), the Jacobian becomes

$$J(e_0) = \begin{bmatrix} 1 + v_1(a - c_1) & 0 \\ 0 & 1 + v_2(a - c_2) \end{bmatrix} \tag{A1}$$

and the two eigenvalues are given by  $\lambda_i = 1 + v_i(a - c_i), i = 1, 2$ . Since  $a > c_i$ , both eigenvalues satisfy condition  $|\lambda_i| > 1$ , and then the point is an unstable node. □

**Proof of Proposition 2.** Inputting  $e_1 = (\frac{a-c_1}{b(1+\omega)}, 0)$  in (12), the Jacobian becomes

$$J(e_1) = \begin{bmatrix} 1 - (a - c_1)v_1 & -\frac{a-c_1}{1+\omega}v_1 \\ 0 & 1 + \frac{a(\epsilon+\omega)+(1-\epsilon)c_1-(1+\omega)c_2}{b(1+\epsilon+2\omega)}v_2 \end{bmatrix} \tag{A2}$$

and the eigenvalues are

$$\begin{aligned} \lambda_1 &= 1 - (a - c_1)v_1, \\ \lambda_2 &= 1 + \frac{a(\epsilon + \omega) + (1 - \epsilon)c_1 - (1 + \omega)c_2}{b(1 + \epsilon + 2\omega)}v_2 \end{aligned} \tag{A3}$$

Simple calculations show that  $|\lambda_2| > 1$  and  $|\lambda_1| < 1$  gives  $0 < v_1 < \frac{2}{(a - c_1)}$ , and then the point  $e_1$  is a saddle point. If  $v_1 > \frac{2}{(a - c_1)}$ , this means that  $|\lambda_i| > 1, i = 1, 2$ ; hence, it an unstable node.  $\square$

**Proof of Proposition 3.** At  $e_*$  the Jacobian becomes

$$J(e_*) = \begin{bmatrix} 1 - \frac{(1 + \omega)(a - 2c_1 + c_2)}{1 + \epsilon + 2\omega}v_1 & -\frac{a - 2c_1 + c_2}{1 + \epsilon + 2\omega}v_1 \\ -\frac{a(\epsilon + \omega) - (1 + \omega)c_2 + (1 - \epsilon)c_1}{1 + \epsilon + 2\omega}v_2 & 1 - \frac{2a(\epsilon + \omega) - 2(1 + \omega)c_2 - 2(1 - \epsilon)c_1}{1 + \epsilon + 2\omega}v_2 \end{bmatrix} \tag{A4}$$

the trace  $T$  and determinant  $D$  take the form

$$\begin{aligned} T &= 2 - \frac{(1 + \omega)(a - 2c_1 + c_2)v_1 + (2a(\epsilon + \omega) - 2(1 + \omega)c_2 + 2(1 - \epsilon)c_1)v_2}{1 + \epsilon + 2\omega}, \\ D &= 1 + \frac{(a - 2c_1 + c_2)(a(\epsilon + \omega) - (1 + \omega)c_2 + (1 - \epsilon)c_1)v_1v_2 - (1 + \omega)(a - 2c_1 + c_2)v_1}{1 + \epsilon + 2\omega} \\ &\quad - \frac{(2a(\epsilon + \omega) - 2(1 + \omega)c_2 + 2(1 - \epsilon)c_1)v_2}{1 + \epsilon + 2\omega} \end{aligned} \tag{A5}$$

According to jury conditions [30], the Nash point becomes locally stable if it satisfies the following:

$$\begin{aligned} 1 - T + D &= \frac{(a - 2c_1 + c_2)[a(\epsilon + \omega) - (1 + \omega)c_2 + (1 - \epsilon)c_1]v_1v_2}{1 + \epsilon + 2\omega} > 0, \\ 1 + T + D &= 4 + \frac{(a - 2c_1 + c_2)[a(\epsilon + \omega) - 2(1 + \omega)c_2 + (1 - \epsilon)c_1]v_1v_2}{1 + \epsilon + 2\omega} \\ &\quad - \frac{2(1 + \omega)(a - 2c_1 + c_2)v_1}{1 + \epsilon + 2\omega} + \frac{4[(1 + \omega)c_2 - (1 - \epsilon)c_1 - a(\epsilon + \omega)]v_2}{1 + \epsilon + 2\omega} > 0, \\ 1 - D &= -\frac{(a - 2c_1 + c_2)[a(\epsilon + \omega) - 2(1 + \omega)c_2 + (1 - \epsilon)c_1]v_1v_2}{1 + \epsilon + 2\omega} \\ &\quad - \frac{(1 + \omega)(a - 2c_1 + c_2)v_1 + 2[(1 + \omega)c_2 - a(\epsilon + \omega) - (1 - \epsilon)c_1]v_2}{1 + \epsilon + 2\omega} > 0 \end{aligned} \tag{A6}$$

It is easy to see that the first conditions in (A6) are always non-negative. Combining the other conditions produces

$$\begin{aligned} 0 &< \frac{-(a - 2c_1 + c_2)[a(\epsilon + \omega) - 2(1 + \omega)c_2 + (1 - \epsilon)c_1]v_1v_2}{1 + \epsilon + 2\omega} + \\ &\quad + \frac{2(1 + \omega)(a - 2c_1 + c_2)v_1 - 4[(1 + \omega)c_2 - (1 - \epsilon)c_1 - a(\epsilon + \omega)]v_2}{1 + \epsilon + 2\omega} < 4 \end{aligned} \tag{A7}$$

and then the Nash point is locally stable.  $\square$

**Proof of Proposition 4.** The eigenvalues for (A4) take the form,

$$\begin{aligned} \lambda_{1,2} &= \frac{1}{2(1 + \epsilon + 2\omega)}(\varphi_1 \pm \sqrt{\varphi_2}), \\ \varphi_1 &= 2(1 + \epsilon + 2\omega) - (1 + \omega)(a - 2c_1 + c_2)v_1 + 2[(1 + \omega)c_2 - (1 - \epsilon)c_1 - a(\epsilon + \omega)]v_2, \\ \varphi_2 &= (1 + \omega)^2(a - 2c_1 + c_2)^2v_1^2 + 4[a(\epsilon + \omega) - (1 + \omega)c_2 + (1 - \epsilon)c_1]^2v_2^2 - \\ &\quad - 4(a - 2c_1 + c_2)(\epsilon + \omega)[a(\epsilon + \omega) - (1 + \omega)c_2 + (1 - \epsilon)c_1]v_1v_2 \end{aligned} \tag{A8}$$

$\square$

**References**

1. Dixit, A. Comparative Statics for Oligopoly. *Int. Rev.* **1986**, *27*, 107–122. [CrossRef]
2. Novshek, W. On the Existence of Cournot Equilibrium. *Rev. Econ. Stud.* **1985**, *52*, 85–98. [CrossRef]

3. Vives, X. *Oligopoly Pricing: Old Ideas and New Tools*; MIT Press: Cambridge, MA, USA, 2001.
4. Singh, N.; Vives, X. Price and Quantity Competition in a Differentiated Duopoly. *RAND J. Econ.* **1984**, *15*, 546–554. [[CrossRef](#)]
5. Askar, S.S.; Abouhawwash, M. Quantity and price competition in a differentiated triopoly: Static and dynamic investigations. *Nonlinear Dyn.* **2018**, *91*, 1963–1975. [[CrossRef](#)]
6. Rand, D. Exotic phenomena in games and duopoly models. *J. Math. Econ.* **1978**, *5*, 173–184. [[CrossRef](#)]
7. Arya, A.; Mittendorf, B.; Sappington, D.E.M. Outsourcing, vertical integration, and price versus quantity competition. *Int. Ind. Organ.* **2008**, *26*, 1–16. [[CrossRef](#)]
8. Puu, T. Chaos in duopoly pricing. *Chaos Solitons Fractals* **1991**, *1*, 573–581. [[CrossRef](#)]
9. Puu, T. The complex dynamics with three oligopolists. *Chaos Soliton Fractals* **1996**, *7*, 2075–2081. [[CrossRef](#)]
10. Tramontana, F. Heterogeneous duopoly with isoelastic demand function. *Econ. Model.* **2010**, *27*, 350–357. [[CrossRef](#)]
11. Naimzada, A.K.; Tramontana, F. Dynamic properties of a Cournot-Bertrand duopoly game with differentiated products. *Econ. Model.* **2012**, *290*, 1436–1439. [[CrossRef](#)]
12. Askar, S.S.; Al-khedhairi, A. Dynamic investigations in a duopoly game with price competition based on relative profit and profit maximization. *J. Comput. Appl. Math.* **2020**, *367*, 112464. [[CrossRef](#)]
13. Askar, S.S. Triopoly Stackelberg game model: One leader versus two followers. *Appl. Math. Comput.* **2018**, *328*, 301–311. [[CrossRef](#)]
14. Ma, J.; Sun, L.; Hou, S.; Zhan, X. Complexity study on the Cournot-Bertrand mixed duopoly game model with market share preference. *Chaos* **2018**, *28*, 023101–023110. [[CrossRef](#)]
15. Askar, S.S. A Dynamic Duopoly Model: When a Firm Shares the Market with Certain Profit. *Mathematics* **2020**, *8*, 1826. [[CrossRef](#)]
16. Elsadany, A.A. Dynamics of a Cournot duopoly game with bounded rationality based on relative profit maximization. *Appl. Math. Comput.* **2017**, *294*, 253–263. [[CrossRef](#)]
17. Cavalli, F.; Naimzada, A.; Tramontana, F. Nonlinear dynamics and global analysis of a heterogeneous Cournot duopoly with a local monopolistic approach versus a gradient rule with endogenous reactivity. *Commun. Nonlinear Sci. Numer. Simul.* **2015**, *23*, 245–262. [[CrossRef](#)]
18. Tremblay, C.H.; Tremblay, V.J. The Cournot-Bertrand model and the degree of product differentiation. *Econ. Lett.* **2011**, *111*, 233–235. [[CrossRef](#)]
19. Fanti, L.; Buccella, D. Corporate social responsibility, profits and welfare with managerial firms. *Int. Rev. Econ.* **2017**, *64*, 341–356. [[CrossRef](#)]
20. Ghosh, A.; Mitra, M. Reversal of Bertrand–Cournot rankings in the presence of welfare concerns. *J. Inst. Theor. Econ.* **2014**, *170*, 496–519. [[CrossRef](#)]
21. Matsumura, T.; Matsushima, N.; Cato, S. Competitiveness and R&D competition revisited. *Econ. Model.* **2013**, *31*, 541–547.
22. Elsadany, A.A.; Awad, A.M. Nonlinear dynamics of Cournot duopoly game with social welfare. *Electron. J. Math. Appl.* **2016**, *4*, 173–191.
23. Kim, S.L.; Lee, S.H.; Matsumura, T. Corporate social responsibility and privatization policy in a mixed oligopoly. *J. Econ.* **2019**, *128*, 67–89. [[CrossRef](#)]
24. Zhou, J.; Zhou, W.; Chu, T.; Chang, Y.X.; Huang, M.J. Bifurcation, intermittent chaos and multi-stability in a two-stage Cournot game with R&D spillover and product differentiation. *Appl. Math. Comput.* **2019**, *341*, 358–378.
25. Cao, Y.; Zhou, W.; Chu, T.; Chang, Y. Global Dynamics and Synchronization in a Duopoly Game with Bounded Rationality and Consumer Surplus. *Int. J. Bifurc. Chaos* **2019**, *29*, 1930031. [[CrossRef](#)]
26. Ahmed, E.; Hegazi, A.S.; Elettrey, M.F.; Askar, S.S. On multi-team games. *Phys. A Stat. Mech. Its Appl.* **2006**, *369*, 809–816. [[CrossRef](#)]
27. Ahmed, E.; Elettrey, M.F. Controls of the complex dynamics of a multi-market Cournot model. *Econ. Model.* **2014**, *37*, 251–254. [[CrossRef](#)]
28. Peng, Y.; Lu, Q. Complex dynamics analysis for a duopoly Stackelberg game model with bounded rationality. *Appl. Math. Comput.* **2015**, *271*, 259–268. [[CrossRef](#)]
29. Tanimoto, J. *Evolutionary Games with Sociophysics*; Springer: Berlin/Heidelberg, Germany, 2019.
30. Tanimoto, J. *Fundamentals of Evolutionary Game Theory and Its Applications*; Springer: Berlin/Heidelberg, Germany, 2015.